AXIN1 bi-allelic variants disrupting the C-terminal DIX domain cause craniometadiaphyseal osteosclerosis with hip dysplasia

Graphical abstract

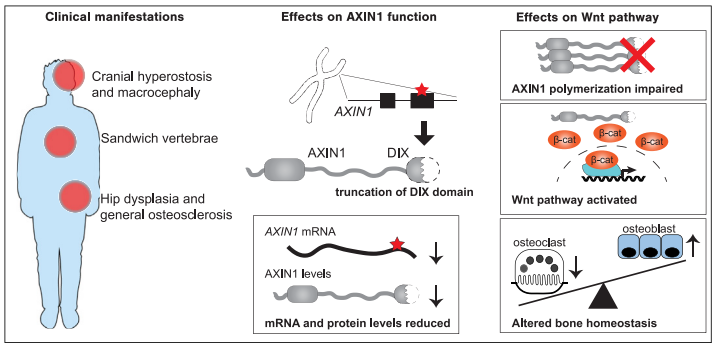

Authors

Paulien Terhal, Anton J. Venhuizen, Davor Lessel, ..., Aida Bertoli-Avella, Madelon M. Maurice, Uwe Kornak

Correspondence

p.a.terhal@umcutrecht.nl (P.T.), uwe.kornak@med.uni-goettingen.de (U.K.)

Terhal et al. describe a sclerosing bone disorder with hip dysplasia due to homozygous truncating variants in *AXIN1* leading to a loss of its C-terminal DIX domain. Analysis of primary and genome-edited cells harboring the variants revealed enhanced basal canonical Wnt pathway activity, which was attenuated by a tankyrase inhibitor.

Terhal et al., 2023, The American Journal of Human Genetics *110*, 1470–1481
September 7, 2023
https://doi.org/10.1016/j.ajhg.2023.07.011

ARTICLE

AXIN1 bi-allelic variants disrupting the C-terminal DIX domain cause craniometadiaphyseal osteosclerosis with hip dysplasia

Paulien Terhal,[1,20,*] Anton J. Venhuizen,[2,20] Davor Lessel,[3,4] Wen-Hann Tan,[5,6] Abdulrahman Alswaid,[7,8] Regina Grün,[9] Hamad I. Alzaidan,[10] Simon von Kroge,[11] Nada Ragab,[9] Maja Hempel,[3,12] Christian Kubisch,[3] Eduardo Novais,[13] Alba Cristobal,[2] Kornelia Tripolszki,[14] Peter Bauer,[14,15] Björn Fischer-Zirnsak,[16] Rutger A.J. Nievelstein,[17] Atty van Dijk,[18] Peter Nikkels,[19] Ralf Oheim,[11] Heidi Hahn,[9] Aida Bertoli-Avella,[14] Madelon M. Maurice,[2] and Uwe Kornak[9,16,*]

Summary

Sclerosing skeletal dysplasias result from an imbalance between bone formation and resorption. We identified three homozygous, C-terminally truncating *AXIN1* variants in seven individuals from four families affected by macrocephaly, cranial hyperostosis, and vertebral endplate sclerosis. Other frequent findings included hip dysplasia, heart malformations, variable developmental delay, and hematological anomalies. In line with AXIN1 being a central component of the β-catenin destruction complex, analyses of primary and genome-edited cells harboring the truncating variants revealed enhanced basal canonical Wnt pathway activity. All three *AXIN1*-truncating variants resulted in reduced protein levels and impaired AXIN1 polymerization mediated by its C-terminal DIX domain but partially retained Wnt-inhibitory function upon overexpression. Addition of a tankyrase inhibitor attenuated Wnt overactivity in the *AXIN1*-mutant model systems. Our data suggest that AXIN1 coordinates the action of osteoblasts and osteoclasts and that tankyrase inhibitors can attenuate the effects of AXIN1 hypomorphic variants.

Introduction

Sclerosing skeletal dysplasias result from increased bone formation by osteoblasts leading to hyperostosis, or a lack of bone resorption by osteoclasts leading to osteopetrosis.[1,2] Canonical Wnt signaling conveyed via the regulation of nuclear β-catenin plays a pivotal role in bone homeostasis, which is evidenced by the large number of skeletal dysplasias with altered bone mass caused by defects in genes playing a role in this pathway.[3] As indicated by the osteogenesis imperfecta-like phenotype caused by bi-allelic loss-of-function variants in *WNT1* (OI15 [MIM: 615220]), WNT1 is an important ligand in bone mass regulation.[4,5] Conversely, overexpression of *Wnt1* in murine osteoblasts elicits a tremendous hyperostosis.[6] Likewise, loss-of-function variants in *LRP5* and *LRP6* encoding co-receptors for the Wnt receptor Frizzled can cause low bone mass disorders (osteoporosis pseudoglioma [MIM: 259770]), while certain gain-of-function variants lead to excessive bone formation (endosteal hyperostosis [MIM: 144750].[7–10] After ligand binding to the Frizzled-LRP5/LRP6 receptor complexes, β-catenin gets stabilized by the inhibition of its destruction complex. The β-catenin destruction complex is a large, multiprotein complex, comprised of the core scaffold proteins APC and AXIN1/2 and kinases GSK3 and CK1 that phosphorylate β-catenin and mark it for proteasomal degradation.[11] While osteoblast differentiation is positively influenced by canonical Wnt signaling at different steps, osteoclast differentiation is prevented by high β-catenin levels.[12] This occurs either through increased expression of osteoprotegerin in osteoblasts or through a direct inhibitory effect of β-catenin in osteoclasts.[13,14]

AXIN1 is the principal coordinator of the β-catenin destruction complex, bringing all its major components in close proximity and thereby vastly accelerating β-catenin phosphorylation.[11,15] AXIN1 harbors an N-terminal regulator of G protein signaling (RGS) domain, a large

[1]Division of Laboratories, Pharmacy and Biomedical Genetics, University Medical Centre Utrecht, 3584EA Utrecht, the Netherlands; [2]Center for Molecular Medicine and Oncode Institute, University Medical Centre Utrecht, 3584CG Utrecht, the Netherlands; [3]Institute of Human Genetics, University Medical Center Hamburg-Eppendorf, 20251 Hamburg, Germany; [4]Institute of Human Genetics, University Hospital Salzburg, Paracelsus Medical University, 5020 Salzburg, Austria; [5]Division of Genetics and Genomics, Boston Children's Hospital, Boston, MA 02115, USA; [6]Harvard Medical School, Boston, MA 02115, USA; [7]Department of Pediatrics, King Abdullah Specialized Children's Hospital, Riyadh 14611, Saudi Arabia; [8]King Saud Bin Abdulaziz University For Health Sciences, Riyadh 22490, Saudi Arabia; [9]Institute of Human Genetics, University Medical Center Göttingen, 37073 Göttingen, Germany; [10]Medical Genetics Department, King Faisal Specialist Hospital and Research Center, Alfaisal University, Riyadh 11211, Saudi Arabia; [11]Department of Osteology and Biomechanics, University Medical Center Hamburg-Eppendorf, 22529 Hamburg, Germany; [12]Institute of Human Genetics, Heidelberg University Hospital, 69120 Heidelberg, Germany; [13]Department of Orthopedic Surgery, Boston Children's Hospital, Boston, MA 02115, USA; [14]Centogene GmbH, 18055 Rostock, Germany; [15]University Hospital Rostock, Internal Medicine, Hemato-oncology, 18057 Rostock, Germany; [16]Institute of Medical Genetics and Human Genetics, Charité-Universitätsmedizin Berlin, 13353 Berlin, Germany; [17]Department of Radiology & Nuclear Medicine, University Medical Centre Utrecht, 3584CX Utrecht, the Netherlands; [18]Expert Center for Skeletal Dysplasia, Wilhelmina Children's Hospital, University Medical Center Utrecht, 3584EA Utrecht, the Netherlands; [19]Department of Pathology, University Medical Centre Utrecht, 3584CX Utrecht, the Netherlands
[20]These authors contributed equally
*Correspondence: p.a.terhal@umcutrecht.nl (P.T.), uwe.kornak@med.uni-goettingen.de (U.K.)
https://doi.org/10.1016/j.ajhg.2023.07.011.

intrinsically disordered region (IDR), and a C-terminal Dvl-Axin-interacting (DIX) domain. The RGS domain interacts with APC, whereas the IDR comprises binding domains for multiple proteins, including β-catenin, GSK3β, and CK1.[16] The DIX domain mediates AXIN1 self-polymerization, which is crucial for efficient destruction complex activity.[17] In addition, in Wnt-activated cells, the DIX domain forms heteropolymers with DVL, which leads to β-catenin stabilization and Wnt pathway activation.[18]

Expression of *AXIN1* is essential for embryonic development. Fruitflies and zebrafish lacking *AXIN1* orthologues *Axn* and *axin1*, respectively, display severe developmental defects.[19,20] In mice, inactivating variants in *Axin1* led to lethality 8–9 days post-coitum.[21] In contrast, targeted inactivation in the osteoblast lineage in mice leads to an osteosclerotic phenotype.[22] AXIN1 polymerization appears to be essential for embryogenesis, since segmentation in *Axn* null fruitfly embryos could be rescued by overexpression of wild-type *Axn* but not by a mutant encoding a polymerization-deficient protein.[23] These results suggest that polymerization-deficient AXIN1 is compromised in its ability to downregulate Wnt/β-catenin signaling in an *in vivo* setting. In humans, somatic *AXIN1* pathogenic variants are known to induce the formation of various types of cancer, most notably hepatocellular carcinoma.[24] In addition, we demonstrated previously that cancer-associated *AXIN1* missense variants affecting the RGS domain can induce Wnt pathway activation in the absence of Wnt ligands.[25]

Despite the large body of information on the consequences of *AXIN1* alterations in multiple model systems, the effects of *AXIN1* germline variants on human development and health are largely unknown. Here, we report on the clinical history of seven individuals from four families harboring C-terminal-truncating, homozygous variants in *AXIN1*. Radiologically, these individuals show a unique combination of hyperostosis and metaphyseal sclerosis in combination with hip dysplasia and variable developmental delay. Functional experiments highlight the effects of these truncating variants on AXIN1 polymerization and Wnt signaling and point to potentially ameliorating effects of a small molecule stabilizing the β-catenin destruction complex.

Material and methods

Participants and genetic analysis

All four families gave written informed consent for genetic testing and agreed to the use of data for research purposes in accordance with the guidelines of the local ethics committees and the Declaration of Helsinki. Affected individuals from all four families were analyzed by exome sequencing in four different centers. Details on the generation of sequencing data and its bioinformatic analysis can be found in supplemental material and methods.

Cell culture

Human skin fibroblasts from individual F2-III-2 and age-matched controls, human embryonic kidney (HEK293T) and HeLa cells were cultured in Dulbecco's modified Eagle's medium with high glucose (Sigma-Aldrich, Taufkirchen, Germany), supplemented with 10% fetal bovine serum (GE Healthcare, Chicago, Illinois, USA), 50 units/mL penicillin, and 50 units/mL streptomycin (Invitrogen). Cells were cultured in 5% CO_2 at 37°C. Wnt3a-conditioned medium was obtained from mouse L-cells stably expressing and secreting Wnt3a. L-cell conditioned medium was obtained from control L-cells. Human skin fibroblasts were stimulated by adding recombinant Wnt3a (Peprotech, Rocky Hill, NJ, USA) to the culture medium to a final concentration of 100 ng/mL. XAV939 (Sigma-Aldrich, Taufkirchen, Germany) was diluted in DMSO and added to the cell cultures at the indicated concentrations.

Constructs

TOPFlash and FOPFlash luciferase reporter plasmids and thymidine kinase (TK)-Renilla and *Axin1b* expression constructs were described previously.[25,26] Variants were introduced by site-directed mutagenesis (see mutagenesis primers in Table S1) via Q5 High-Fidelity 2X Master Mix (NEB, Frankfurt am Main, Germany) supplemented. SpCas9(BB)-2A-Puro (PX459) V2.0 plasmid was obtained from Addgene. Guide RNAs were cloned into this vector according to protocol (see Table S1 for guide sequences including overhangs).[27] A doxycycline-inducible Cas9 lentiviral construct was obtained from Addgene (#87360). Guide RNAs were cloned, as mentioned before, with BsmBI instead of BbsI in the Golden Gate assembly step.

Antibodies

The following primary antibodies were used for immunoblotting (IB) and immunofluorescence (IF): mouse-anti-actin (MP Biomedicals, #08691001, 1:10,000), rabbit-anti-actin (Cell Signaling Technologies, 13E5, 1:5,000), goat-anti-AXIN1 (R&D systems, AF3287, 1:1,000), rabbit-anti-AXIN1 (Cell Signaling Technologies, C76H11, 1:500), and rabbit-anti-non-phospho-β-Catenin Ser33/37/Thr41 (Cell Signaling Technologies, D13A1, 1:1,000). Secondary antibodies used for IB were as follows: donkey-anti-goat Alexa 680 (Invitrogen, 1:8,000) and goat anti-rabbit-IgG-HRP (Santa Cruz Biotechnology, sc-2004, 1:10,000). Secondary antibodies used for IF were as follows: donkey-anti-goat Alexa 488 (Invitrogen, 1:8,000).

Lentiviral transduction

Lentiviral particles were generated with HEK293T cells transfected with 15 μg of iCas9 vector, 7.5 μg psPAX2, and 7.5 μg pMD2G plasmids with a 1:3 ratio of DNA to polyethyleneimine (PEI). Lentivirus was collected 2 days after transfection and filtered with a 0.45 μm filter. HEK293T cells were seeded in six-well plates and transduced with 500 μL virus and 8 μg/mL polybrene. Selection with 2 μg/mL puromycin was started 48 h after transduction and maintained. For Cas9 induction, lines were treated with 1 μg/mL doxycycline for 3 days.

Transfection PX459 plasmid and genotyping

HEK293T cells were transfected with 500 ng PX459 plasmid and 10 pmol repair oligo via FuGene 6 (Promega, Leiden, the Netherlands) according to manufacturer's protocol. After 2 days, selection with 2 μg/mL puromycin was started for 2 days. Genomic DNA was isolated with the DNA Micro Kit (Quiagen, Hilden, Germany) according to protocol. Bulk sequencing was performed with primers in Table S1 with Taq polymerase (NEB,

Frankfurt am Main, Germany). PCR products were isolated from gel and sent for Sanger sequencing with the sequencing primers indicated in Table S1. Editing efficiency was predicted via the Synthego CRISPR analysis tool. Successfully edited bulk populations were diluted to one cell per 96-well. Clones that grew out as single colonies were genotyped as described above.

TOPFlash luciferase reporter assay

HEK293T cells were cultured in 24-well plates and transfected the next day with FuGene 6 (Promega, Leiden, the Netherlands) according to manufacturer's protocol. Cells were transfected with a total amount of 250 ng plasmid per well consisting of the construct of interest, 30 ng of TOPFlash or FOPFlash reporter construct, 5 ng of thymidine kinase (TK)-Renilla, and empty vector. Clonal lines were transfected with 30 ng TOPFlash or FOPFlash and 5 ng of thymidine kinase (TK)-Renilla. 6 h post-transfection, cells were stimulated with Wnt3a-conditioned medium (CM) or L-cell CM and incubated overnight. The next day, cells were lysed with 1X Passive Lysis Buffer (Promega, Leiden, the Netherlands) for 20 min at room temperature. Firefly Luciferase and Renilla were measured on a Berthold luminometer Centro LB960 with the Dual Luciferase Reporter Kit (Promega). Lysates were used for immunoblot analysis.

Immunofluorescence and confocal microscopy

HEK293T and HeLa cells were grown on glass coverslips in 24-well plates (coated with laminin). After overnight transfection of 100 ng of AXIN1 per well, cells were fixed in 4% paraformaldehyde (PFA) in 50 mM sodium phosphate, pH 7.4, buffer. After being quenched in 50 mM NH_4Cl and blocked with 2% BSA and 0.1% saponin in PBS, cells were incubated for 1 h with the primary antibody followed by three washes and incubation with secondary antibody and DAPI for 45 min. Cells were mounted in Prolong Diamond (Invitrogen). Images were acquired with a LSM700 confocal microscope (Zeiss, Nussloch, Germany) and analyzed with ImageJ. Thresholds were adjusted with the "Intermodes" treshold parameter. Particles of size >0.01 μm^2 were included. No filtering on circularity was performed. For quantification of total cell fluorescence intensity, ImageJ software was used. To correct for background signal, average intensity of a neighboring area was determined and multiplied by the area of the cell. This background intensity was subtracted from the integrated density of each cell.

Immunoprecipitation

The different HEK293T AXIN1-truncating clones were seeded in 15 cm dishes (Corning) at 40% confluency. The following day, cells were resuspended in 2 mL lysis buffer (50 mM Tris [pH 7.5], 150 mM NaCl, 0.5% Triton X-100, 10% glycerol, 5 mM EDTA, 1 mM DTT, 50 mM sodium fluoride, and protease inhibitors aprotinin [10 μg/mL], leupeptin [10 μg/mL], and sodium vanadate [100 μM]). Cells were lysed for 30–45 min at 4°C and subsequently centrifuged for 20 min at 14,000 rpm at 4°C. Samples were taken to compare protein input levels. For AXIN1 immunoprecipitation, 1 μg per sample of goat-AXIN1 antibody was added to each lysate, followed by incubation overnight while tumbling at 4°C. 20 μL of protein G-coupled beads (Millipore, Sigma-Aldrich, Taufkirchen, Germany) were washed three times with lysis buffer. Subsequently, proteins were eluted in 2× sample buffer (SDS, β-mercaptoethanol, glycerol, Tris [pH 6.8], bromophenol blue) and boiled for 6 min at 90°C.

SDS PAGE and Immunoblotting of HEK293 cells

Proteins were separated on the basis of molecular weight by SDS-PAGE with 10% polyacrylamide. After separation, proteins were transferred to a polyvinylidene fluoride (PVDF) membrane (Immobilon-F) (Millipore, Sigma-Aldrich, Taufkirchen, Germany). After membrane blocking by Odyssey Blocking Buffer (Li-Cor, diluted 1:1 in TBS), membranes were incubated with primary antibody overnight at 4C. After washing with Tris-buffered saline containing 0.5% Tween (TBS-T), membranes were incubated with secondary antibody for 60 min. After additional washing steps with TBS-T and TBS, membranes were scanned by a Typhoon Biomolecular Imager (GE Healthcare, Chicago, Illinois, USA).

Immunoblot of human skin fibroblasts from individual F2-III-2

Human fibroblasts were lysed in RIPA buffer (150 mM NaCl, 50 mM Tris, 5 mM EDTA, 1% Triton X-100, 0.25% deoxycholate, and 0.1% SDS) with Halt protease inhibitor cocktail (Thermo Fisher Scientific, Kandel, Germany) and phosSTOP phosphatase inhibitor (Roche, Mannheim, Germany). Protein concentrations were analyzed with the BCA-kit (Thermo Fisher Scientific, Kandel, Germany). 20 μg (β-Catenin) or 50 μg (Axin1) protein per lane was separated with 4%–20% gradient gel (Bio-Rad). After blotting, PVDF membranes were blocked in 5% milk/TBST and probed with primary antibodies diluted in 2.5% milk/TBST or 2% BSA/Azid and detected with HRP-conjugated secondary antibodies followed by visualization by ECL reagent (PerkinElmer, Waltham, MA, USA).

RNA extraction from affected-individual-derived fibroblasts

Cultured fibroblasts were lysed in Trizol (Life Technologies, Bleiswijk, the Netherlands) and total RNA was extracted via the Direct-Zol RNA Miniprep Kit (ZymoResearch Europe, Freiburg, Germany). cDNA was transcribed with the RevertAid H Minus First Strand cDNA Synthesis Kit (Thermo Fisher Scientific, Kandel, Germany).

Quantitative real-time PCR

RNA was harvested from HEK293T cells with the RNeasy Kit (Qiagen, Hilden Germany) according to manufacturer's protocol. DNA was removed with RNase-Free DNase (Qiagen, Hilden Germany). Reverse transcriptase reactions were performed with either the iScript cDNA synthesis kit (Biorad) with 500 ng RNA input or with the RevertAid H Minus First Strand cDNA Synthesis Kit (Thermo Fisher Scientific, Kandel, Germany) with 1 μg RNA input. Quantitative real-time PCR was performed with a Biorad CFX96 or a Quant Studio 5 (Thermo Fisher Scientific, Kandel, Germany). See Table S1 for used primers.

Bone histological sections and histomorphometry

During epiphysiodesis at the left knee of individual F1-II-1, a core bone biopsy from the distal femur was taken, immediately fixed in 3.5% formalin, and subsequently decalcified. Specimens were embedded in paraffin, cut in 4 μm thick sections, and stained with toluidine blue. To evaluate the microstructure and cellular characteristics, an Osteomeasure system (OsteoMetrics, Decatur, USA) was used. Bone volume per tissue volume (BV/TV, %), trabecular thickness (Tb.Th, μm), and trabecular number (Tb.N, 1/μm) as well as the amount of osteocytes per bone area (N.Ot/B.Ar, 1/mm^2)

were determined and compared to a healthy age- and sex-matched control of the distal femur.

Statistical analysis

Data were plotted and statistically evaluated with GraphPad Prism (GraphPad, San Diego, CA). For comparison of normalized densitometry and gene expression values in two samples, we used a Mann-Whitney test. We performed a Kruskall-Wallis test to determine the significant differences in area and roundness between multiple non-normally distributed conditions in the immunofluorescence microscopy images. Gene expression in more than two samples was statistically analyzed by a one-way ANOVA test.

Results

By exome sequencing, we identified homozygous truncating variants in the region of *AXIN1* encoding the C-terminal part of AXIN1 in seven individuals with osteosclerosis from four families (Figures 1A and S1). In family 1, a homozygous duplication variant in *AXIN1* (*AXIN1a*: c.2503dupG [p.Val835Glyfs*4] [GenBank: NM_003502.3]; *AXIN1b*: c.2395dupG [p.Val799Glyfs*4] [GenBank: NM_181050.3]) was detected in the two affected sisters. Both parents and unaffected sisters (individual F1-II-2 and F1-II-3) were heterozygous carriers. *AXIN1* has two splice variants: *AXIN1a* consists of 11 coding exons, while coding exon 9 (108 bp) is spliced out in *AXIN1b*. The transcription of both splice variants has been experimentally validated.[28] We will refer to the shorter *AXIN1b* variant (GenBank: NM_181050.3) throughout this manuscript. By GeneMatcher (https://genematcher.org/), we identified two other families. The male individual in family 2 was homozygous for the c.2167C>T (p.Arg723*) variant, while family 3 showed a homozygous nonsense variant c.2413C>T (p.Arg805*) in the proband and a heterozygous variant in the mother (DNA from the father was not available). Through our collaborative network, we identified three additional individuals harboring a homozygous c.2167C>T (p.Arg723*) variant from family 4 (Table 1). Notably, homozygous loss-of-function variants are completely absent from the gnomAD dataset comprising unaffected individuals.[29]

Clinical and radiological features

The age of the affected individuals was between 3 months and 15.5 years (clinical description in Table 1 and supplemental note). Most individuals had macrocephaly ranging from +2.2 to +6.1 SD, while two individuals showed relative macrocephaly. All displayed hypertelorism with a low nasal bridge. Longitudinal growth was significantly impaired in three individuals and borderline in one individual. The skeletal phenotype affected the cranial, axial, and appendicular skeleton (Figures 1B–1G, S2, and S3). Skull radiographs and CT images showed sclerosis at the base of the skull and a progressive thickening of the calvarial bone beginning in the first year of life (Figures 1B and 1C). Osteodensitometry in adolescent female individuals F1-II-1 and F1-II-4 revealed a *Z* score of 8.6 and 6.6 of the lumbar spine, respectively. Bone densitometry in the heterozygous family members was mildly increased (*Z* score of 3.5 of the lumbar spine in the mother, 1.7 and 1.4 in the siblings). Spine radiographs showed a sclerotic rim of vertebrae at younger ages, which developed into sclerotic endplates with sandwich appearance in adolescence (Figures 1D and 1E). Five of six individuals had hip dysplasia with frequent luxations requiring multiple operations (Figure 1F). Flaring of the femora indicating a modeling defect was visible at all stages (Figure 1G). In addition, variable opacity of the distal femoral metaphysis was evident, which in one individual appeared striated. Also, in other radiographs coarse trabeculation was found. Furthermore, there was evidence for mild cortical thickening. Development was globally delayed in individuals F2-III-2, F4-III-1, F4-III-3, and F4-III-4, harboring the p.Arg723* variant, and unremarkable in the three other individuals, except for selective mutism in the two sisters from family 1. Cardiac involvement was noted in three individuals: in one, a patent ductus arteriosus, and in the other two, a complex malformation with atrial and ventricular septal defects. Individuals F2-III-2, F4-III-1, and F4-III -3 suffered from pancytopenia with recurrent infections, partially requiring transfusions. In summary, this sclerosing skeletal dysplasia combines aspects of osteopetrosis (sandwich vertebrae, metaphyseal flaring) and of endosteal hyperostosis (calvarial and cortical thickening).

Bone histology and turnover markers

We determined bone turnover markers in the affected females from family 1. Compared to three age- and sex-matched controls and standard values, a tendency toward lower RANKL/OPG ratios and elevated P1NP levels were observed (Table S2). Radiographs show a metaphyseal accumulation of coarse trabeculae in many individuals (Figures 2A and 2B). A bone biopsy from individual F1-II-1 was collected during elective surgery at the age of 14.5 years. Histological examination showed a broad primary spongiosa near the epiphyseal plate with thickened and abundant trabeculae (Figures 2C and 2D). Histomorphometry underlined an increased bone volume fraction, an elevated bone remodeling, and an accumulation of osteocytes embedded within the bone matrix (Figure S4). These results imply high osteoblast activity.

Effects of AXIN1 variant p.Arg723* on protein abundance and gene regulation in individual F2-III-2

Since variant c.2167C>T locates to the third last exon of *AXIN1*, the resulting nonsense variant p.Arg723* may trigger nonsense-mediated decay. However, as complete loss of *Axin1* has lethal effects in mice, residual function of a C-terminally truncated protein seemed likely.[21] We performed immunoblots by using an antibody recognizing an N-terminal AXIN1 epitope. In healthy control fibroblast lysates, a band of approximately 110 kDa was detected (Figure 3A). By contrast, skin fibroblasts from individual

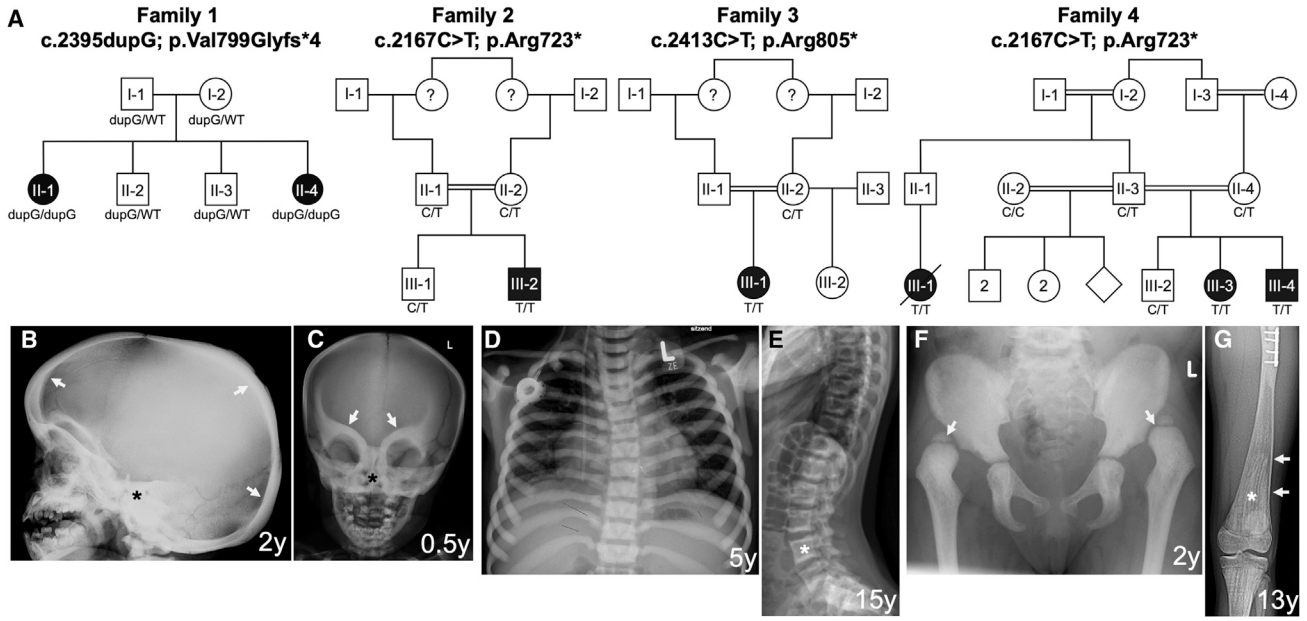

Figure 1. Pedigrees, genetic findings, and radiological phenotype of a sclerosing skeletal dysplasia with hip dysplasia and variable developmental delay

(A) Pedigrees of the four families with identified *AXIN1* pathogenic variants and segregation analysis.

(B–G) Representative radiographs (for more details consult Figure S2).

(B) Lateral skull radiograph of individual F1-II-4 at 2 years of age showing calvarial thickening (arrows) and sclerosis of skull and skull base (*).

(C) Frontal skull radiograph of individual F4-III-3 at 6 months of age. Note sclerotic rim around orbitae (arrows) and sclerotic skull base (*).

(D) Chest radiograph of individual F2-III-2 at 5 years of age demonstrating sclerosis of vertebrae and ribs.

(E) Lateral spine radiograph of individual F3-III-1 at age 15 years. Note sclerotic vertebral endplates leading to a sandwich appearance (*).

(F) Radiograph of the pelvis of individual F1-II-1 at 2 years of age showing hip dysplasia and luxation (arrows), delayed epiphyseal ossification of the femoral head, sclerosis, broadened femoral necks, and endosteal cortical thickening of the femoral diaphysis.

(G) Knee and femur radiograph of individual F1-II-1 at 13 years of age displaying metaphyseal flaring indicating a modeling defect (arrow) and metaphyseal striation (*).

F2-III-2 displayed a band of approximately 100 kDa at 20% intensity. The *AXIN1* mRNA was similarly reduced while no significant change in *TNFRSF11B* expression (coding for OPG) was detected (Figures S5A and S5B). Thus, residual *AXIN1* mRNA expression gives rise to low levels of a stable truncated protein. Expression of *AXIN1*-paralogue *AXIN2* is known to be regulated by canonical Wnt signaling.[30] At basal cell culture conditions, we found *AXIN2* expression to be elevated in skin fibroblasts of F2-III-2 (Figure 3B). In addition, non-phosphorylated β-catenin protein levels were elevated in these cells (Figure 3C). These findings indicate enhanced canonical Wnt pathway activity in fibroblasts with reduced amounts of truncated AXIN1.

C-terminally truncated AXIN1 fails to assemble properly

Upon overexpression of *AXIN1*, AXIN1 forms DIX domain-mediated cytosolic protein assemblies often referred to as puncta.[17] On the basis of the crystal structure of the DIX domain, we anticipated that AXIN1 variants p.Arg723*, p.Val799Glyfs*4, and p.Arg805* may affect DIX domain integrity and puncta formation (Figure S6A). To investigate this, we overexpressed these variants in HeLa cells, HEK293T cells (Figure 4), and AXIN1-deficient HEK293T cells (Figure S6B). AXIN1 WT formed puncta with diameters up to 1 μm, as previously described.[31] By contrast, AXIN1 p.Arg723* was incapable of forming such structures, displaying a diffuse cytosolic localization. Furthermore, AXIN1 variants p.Val799Glyfs*4 and p.Arg805* formed smaller, non-spherical puncta in both cell lines (Figures 4B, S6C, and S6D). Imaging analysis indicated no reduction in total fluorescence, thereby excluding a reduction in AXIN1 levels as the basis of impaired polymerization of truncated AXIN1 variants (Figure S6E). Together, these results indicate that the polymerization capacity of AXIN1-truncating variants p.Arg723*, p.Val799Glyfs*4, and p.Arg805* is compromised.

C-terminally truncated human AXIN1 variants display defects in Wnt pathway suppression

To determine the consequences of *AXIN1*-truncating variants at the physiological level, we used CRISPR-Cas9 in HEK293T cells to introduce variant c.2167C>T (p.Arg723*) in exon 8 through homology-directed repair and mimicked the variants c.2395dupG (p.Val799Glyfs*4) and c.2413C>T (p.Arg805*) in exon 10 by introducing frameshift mutations (Figures S7A–S7C).[27] After clonal dilution, we isolated three clones for p.Arg723* and two

Table 1. Clinical and radiological features of the affected individuals

	Family 1, II-1 (F1-II-1)	Family 1, II-4 (F1-II-4)	Family 2, III-2 (F2-III-2)	Family 3, III-1 (F3-III-1)	Family 4, III-1 (F4-III-1)	Family 4, III-3 (F4-III-3)	Family 4, III-4 (F4-III-4)
AXIN1 variant cDNA (GenBank: NM_181050.3)	c.2395dupG	c.2395dupG	c.2167C>T	c.2413C>T	c.2167C>T	c.2167C>T	c.2167C>T
Coding exon (total 9)	9	9	7	9	7	7	7
Polypeptide	p.Val799Glyfs*4	p.Val799Glyfs*4	p.Arg723*	p.Arg805*	p.Arg723*	p.Arg723*	p.Arg723*
Genomic DNA (hg19)	chr16: g.338208dup	chr16: g.338208dup	chr16: g.343507G>A	chr16: g.338190G>A	chr16: g.343507G>A	chr16: g.343507G>A	chr16: g.343507G>A
Zygosity	homozygous	homozygous	homozygous	homozygous	homozygous	homozygous	homozygous
Sex	F	F	M	F	F	F	M
Age (years)	15.5	8.4	7.1	15.5	3	3	0.25
Height (SD)	158.2 (−1.41 SD)	131.2 (−0.44 SD)	113.5 (−1.9 SD)	160.6 (−0.25 SD)	85 (−2.95 SD)	79 (−3.87 SD)	49 (−4.3 SD)
OFC (SD)	+2.2 SD	+2.5 SD	+3.4 SD	+6.1 SD	N/A	+1.3 SD	+1.7 SD
Development	temporary selective mutism	selective mutism	global developmental delay	normal	global developmental delay	global developmental delay	motor developmental delay
Hypertelorism	yes	yes	yes	yes	yes	yes	yes
Low nasal bridge	yes	yes	yes	yes	yes	yes	yes
Hip dysplasia/luxation	yes	yes	no	yes	yes	yes	N/A
Cardiac	patent ductus arteriosus	normal	ASD, VSD	normal	normal	normal	ASD, VSD
Hematological	no	mild anemia	pancytopenia, transfusions	normal	pancytopenia, transfusions, dyserythropoietic changes	pancytopenia, transfusions	mild anemia
Imaging results							
Calvarial thickening	yes	yes	no (at 4 weeks)	yes	yes	yes	N/A
Sandwich vertebrae	yes	yes	yes	yes	yes	yes	N/A
Cortical thickening	yes	yes	N/A	yes	yes	yes	N/A
Metaphyseal flaring	yes	yes	N/A	N/A	N/A	yes	N/A
Coarse trabeculae	yes	yes	yes	yes	yes	yes	N/A
Brain imaging	mild pachygyria with thick frontal/ temporal cortex, choanal stenosis	calcified cephalic hematoma	ectopic pituitary gland, corpus callosum hypoplasia	arachnoid cyst middle cranial fossa	brain atrophy	N/A	normal
Ultrasound abdomen	normal	normal	bilateral duplex kidneys	mild hepatomegaly	hepatomegaly	N/A	normal

SD, standard deviation; OFC, occipitofrontal circumference; ASD, atrium septum defect; VSD, ventricular septal defect; N/A, not ascertained.

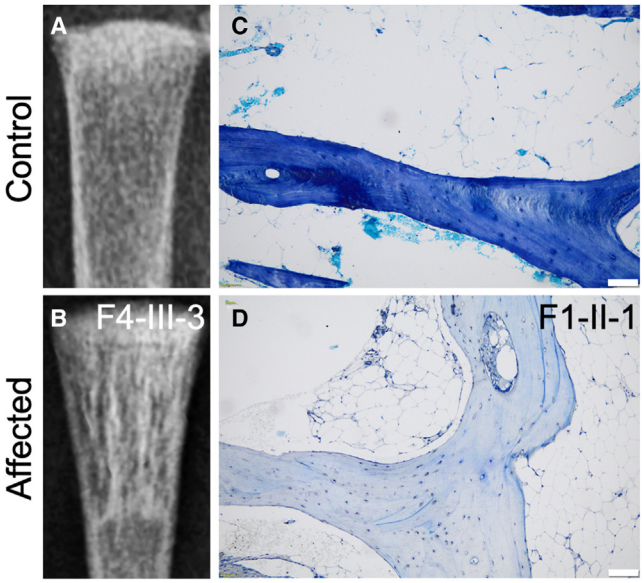

Figure 2. Trabecular bone changes
(A and B) Radiographs of the distal radius of an unaffected age-matched control (A) and from individual F4-III-3 (age 6 months) (B) demonstrate a metaphyseal accumulation of coarse trabeculae. (C and D) Histological analysis (toluidine blue staining) of a femoral bone biopsy from a healthy age- and sex-matched control (C) in comparison to individual F1-II-1 at age 14.5 years (D) confirming persistent trabecular thickening. Scale bars represent 100 μm.

clones carrying *AXIN1* variants p.Asp796Glufs*6 (c.2388_2389del) (*AXIN1b*) and p.Asp796Glufs*7 (c.2387dupA) (*AXIN1b*) (Figure S7C). To assess the effects of these variants at the protein level, we performed immunoprecipitation (IP) by using an AXIN1-specific antibody (Figures 5A and 5B). Protein abundance of the truncated AXIN1 variants was decreased in comparison to the AXIN1 wild-type (WT) control.

We then determined the effects of these variants on Wnt pathway activation by a β-catenin-dependent luciferase assay (Figure 5C). All *AXIN1*-mutant clones displayed basal activation of the Wnt pathway. Of note, we observed clonal variation in the levels of pathway activity between the different clones, which is most likely due to the inherent genetic instability of HEK293T cells (Figure 5C). Increased expression of Wnt target *AXIN2* was evident in some of the clones (Figure S7D). To limit the possibility that CRISPR-Cas9-edited HEK293T cells adapt to these variants over time, we employed a doxycycline-inducible system expressing Cas9 and a gRNA targeting *AXIN1* exon 10. Upon 3 days of doxycycline treatment, an estimated 29% of the bulk population harbored frameshift variants in the desired DNA region (Figure S7E). Luciferase assay analysis of this bulk population indicated an overall 7-fold increase in basal pathway activation compared to iCas9 control cells (Figure S7F). Together, our results suggest that truncating *AXIN1* variants lead to reduced AXIN1 levels and induce hyperactivation of Wnt signaling.

C-terminally truncated AXIN1 variants are subjected to partial nonsense-mediated decay

Increased destabilization of the different truncated AXIN1 variants may be a result of increased protein turnover or decreased mRNA stability due to nonsense-mediated decay (NMD). By quantitative real-time PCR, we observed an overall decrease in *AXIN1* mRNA levels for all *AXIN1*-mutant HEK293T clones in comparison to the original HEK293T cell line and an AXIN1 WT clone (Figure 5D). These results are in line with results obtained in p.Arg723* fibroblasts (Figure S5A) and indicate that premature stop codons in *AXIN1* exons 8 and 11 lead to partial NMD.

Tankyrase inhibitors suppress AXIN1 variant-induced Wnt pathway activation

AXIN1-truncating variants remained capable of Wnt pathway suppression when overexpressed in HEK293T AXIN1 WT and AXIN1 KO cells (Figure S8), indicating that enhancing concentrations of these variants might provide a strategy to restore suppressor activity. We tested this hypothesis by treatment of our *AXIN1*-mutant clones by blocking the enzymatic activity of the poly-ADP-ribosylating enzymes tankyrase 1 and 2 regulating the proteasomal breakdown of AXIN1 and AXIN2.[32] Indeed, treatment of HEK293T AXIN1 p.Arg723* and p.Asp796Glufs*6 cell lines with 100 nM and 1 μM XAV939 led to a dosage-dependent suppression of Wnt pathway activation (Figure 5E). This effect appeared partially attributable to stabilization of AXIN2, since XAV939 was also capable of suppressing aberrant pathway activation in AXIN1 KO cells. In conclusion, tankyrase inhibitors might be able to rescue the effect of AXIN1 truncations, but whether their application *in vivo* is a valid option has to be addressed in future studies.

Discussion

In this report, we describe seven individuals from four families harboring homozygous truncating variants in the last exons of *AXIN1* encoding the C-terminal DIX domain. All affected individuals have skeletal manifestations combining features of osteopetrosis and hyperostosis in combination with dysmorphic features (hypertelorism) and macrocephaly. Further frequent clinical signs were hip luxation, anemia or pancytopenia, and cardiac malformations. Developmental delay, albeit of different degrees, was present in all but one individual. Despite reduced *AXIN1* mRNA levels in fibroblasts, truncated AXIN1 was still produced. All AXIN1-truncated variants displayed a compromised polymerization capacity, indicating a defect in DIX domain function. Moreover, genome-editing-mediated introduction of these AXIN1 variants in HEK293T cells indicated decreased protein levels of the truncated AXIN1 variants and, consequently, enhanced β-catenin activity.

Phenotypically, there is overlap with other disorders caused by variants affecting Wnt pathway components,

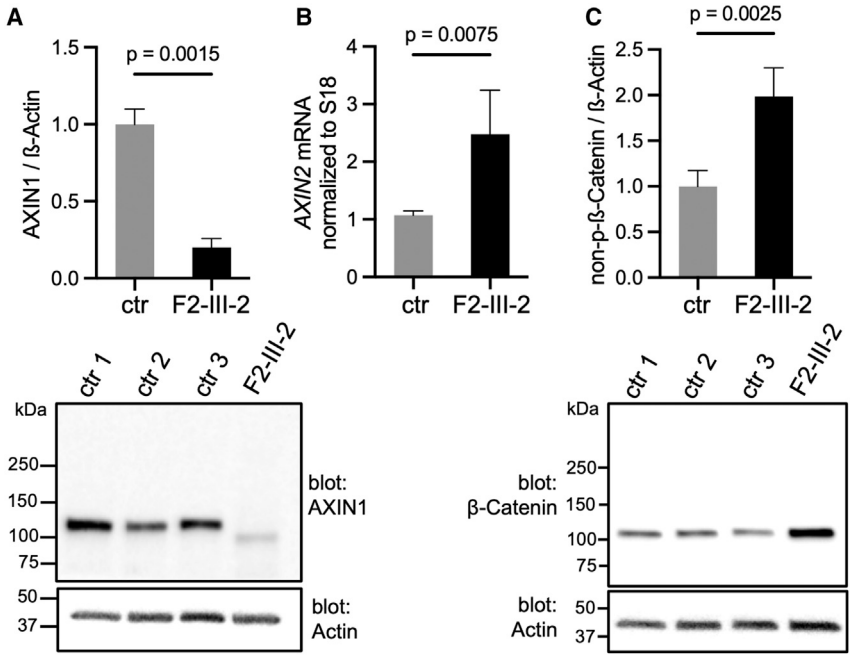

Figure 3. Effects of the pathogenic AXIN1 variant p.Arg723* in skin fibroblasts

(A) AXIN1 immunoblot of lysates from skin fibroblasts from individual F2-III-2 harboring the p.Arg723* variant and matched controls (ctr) (n = 4) cultured under standard conditions. Note shifted band with 80% reduced intensity as indicated in the bar diagram.

(B) Quantitative real-time PCR for *AXIN2* expression normalized to S18 rRNA in fibroblasts from F2-III-2 in comparison to matched controls (ctr) (n = 4).

(C) Immunoblot with antibody against active, non-phosphorylated β-catenin. Lysates are from skin fibroblasts cultured under standard conditions. The quantification indicates elevated canonical Wnt signaling. p values were determined by a Mann-Whitney test. Error bars represent standard error of the mean.

especially with X-linked osteopathia striata with cranial sclerosis (OS-CS [MIM: 300373]) due to *AMER1* variants and with the *DVL1*-related osteosclerotic form of Robinow syndrome (DRS2 [MIM: 616331]). Besides overlapping skeletal manifestations (macrocephaly with cranial sclerosis and sclerosis of long bones), affected individuals with OS-CS also display a predisposition for cardiac anomalies (e.g., patent ductus arteriosus), genitourinary anomalies, and hearing loss.[33–35] Histological examination of an iliac biopsy in a female affected with *AMER1*-linked OS-CS and high-resolution peripheral quantitative computed tomography (HR-pQT) in four individuals with *DVL1*-related Robinow syndrome revealed a similar profile as in our study with increased trabecular bone mineral density and thickness.[36,37]

However, neither these overlapping Wnt-related disorders nor high bone mass phenotypes caused by activating variants in *LRP5* or *LRP6* present with sandwich vertebrae or pronounced metaphyseal sclerosis. This aspect of the phenotype overlaps with autosomal dominant osteopetrosis type

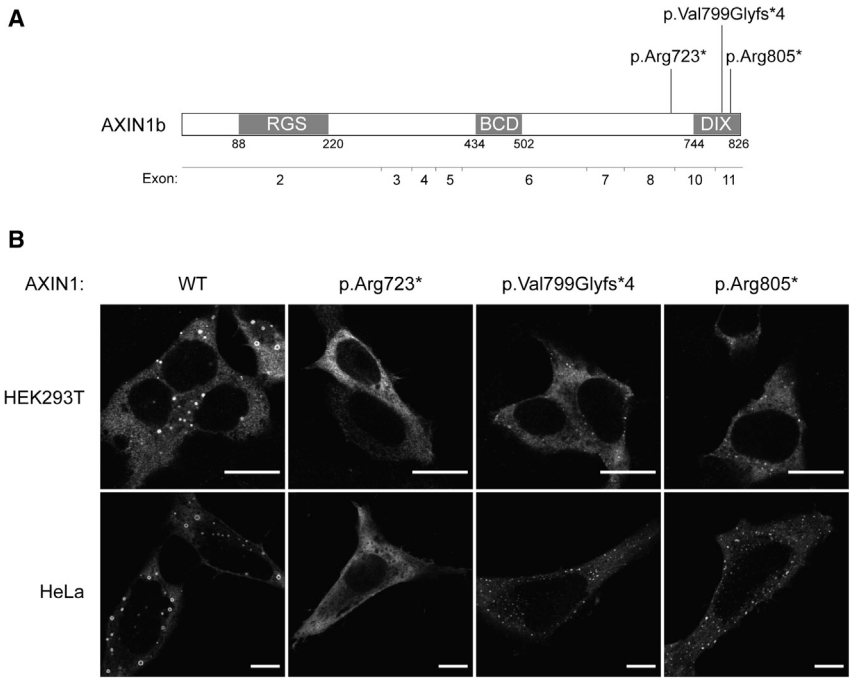

Figure 4. C-terminally truncated AXIN1 fails to assemble properly

(A) Schematic representation of the AXIN1 isoform 1b, which consists of an N-terminal RGS domain, a C-terminal DIX domain, and an intrinsically disordered middle region (IDR) with binding sites for many proteins, including β-catenin via the β-catenin-binding domain (BCD). The respective exons are indicated below the protein structures. Exon 9, exclusive to isoform AXIN1a, is omitted in this schematic.

(B) Immunofluorescence images of HEK293T and HeLa cells overexpressing constructs encoding AXIN1 wild type (WT) and truncating variants p.Arg723*, p.Val799Glyfs*4, and p.Arg805*. Confocal microscopy performed of cells immunofluorescence-labeled with AXIN1 antibody (grayscale). Scale bars represent 10 μm.

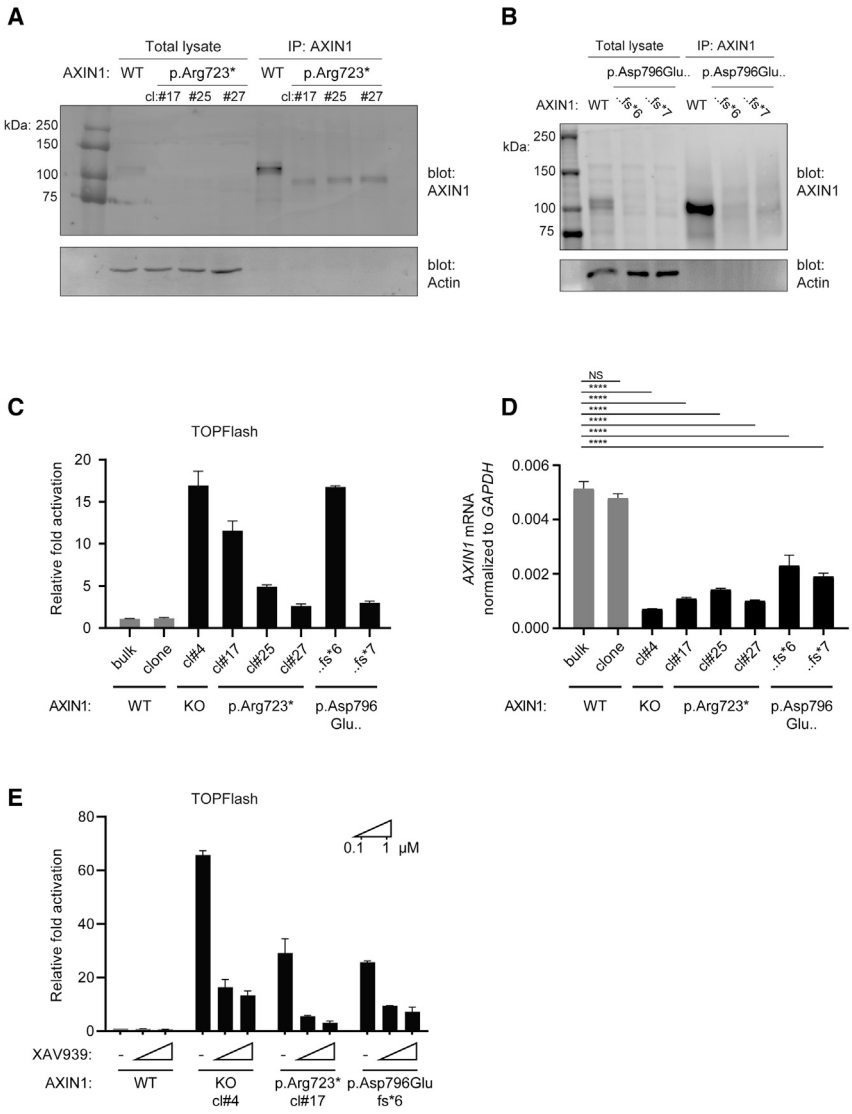

Figure 5. CRISPR-Cas9-introduced *AXIN1* variants lead to protein destabilization and increased Wnt pathway activation

(A and B) Immunoblotting for immunoprecipitation of AXIN1 WT versus p.Arg723*-harboring HEK293T clones and of (B) AXIN1 WT versus variants p.Asp796Glufs*6 and p.Asp796Glufs*7. AXIN1 was poorly detected in the *AXIN1* exon 10-mutant lines. Actin was stained as input control in both experiments.

(C) β-catenin-responsive luciferase-reporter assay including different *AXIN1*-mutant HEK293T clones, which shows Wnt pathway activation in the clones with AXIN1 p.Arg723* or p.Asp796 variants. Graph shows average and standard deviation of luciferase activity in duplicate cell cultures transfected in parallel.

(D) Quantitative real-time PCR hints toward decreased *AXIN1* mRNA levels in HEK293T cells harboring truncating AXIN1 variants. mRNA levels were normalized to *GAPDH*. Error bars represent the standard deviation of three independent biological replicates. One-way ANOVA was performed to determine statistical significance between the HEK293T control cell line and all other conditions. NS indicates that the difference is not statistically significant, p value > 0.05. **** indicates $p < 0.0001$.

(E) β-catenin-responsive luciferase-reporter assay including different *AXIN1*-mutant HEK293T clones after 16 h of treatment with tankyrase inhibitor XAV939. XAV939 treatment rescues variant-induced pathway activation in a concentration-dependent manner. Graph shows average and standard deviation of luciferase activity in duplicate cell cultures transfected in parallel.

2 (Albers-Schönberg disease, ADO2 [MIM: 166600]), which is due to defective osteoclasts.[38,39] Thus, the *AXIN1*-related sclerosing skeletal dysplasia described here shows a unique combination of hyperostosis due to increased osteoblast activity in combination with signs of attenuated osteoclast function, at least at the growth plates. Remarkably, another typical sign of osteopetrosis, increased bone fragility ("marble bone disease"), is not noted in the affected individuals reported here. Probably, the osteoblast-stimulating effect of the AXIN1 truncation sufficiently increases bone quality. The three most severely affected individuals from our series harboring the recurrent, most N-terminally located truncating variant, also suffer from pancytopenia. Impaired bone marrow function and extramedullary hematopoiesis leading to hepatosplenomegaly is often observed in autosomal recessive osteopetrosis (ARO [MIM: 259700]), which however, is attributed to bone marrow obstruction. Therefore, the pancytopenia in our individuals could be a primary effect of altered canonical Wnt signaling in the hematopoietic lineage or niche.

β-catenin in mesenchymal stem cells is important for osteoblast differentiation and leads to upregulation of osteoprotegerin thereby inhibiting osteoclastogenesis, although a direct inhibitory effect on osteoclasts has been shown as well.[13,14,40,41] Additionally, β-catenin expression in osteoblasts leads to downregulation of the pro-osteoclastic RANKL.[42] A conditional knockout of *Axin1* in murine osteoblasts was shown to drive β-catenin accumulation. Consequently, these mice exhibited a lower Rankl/Opg ratio in bone tissue, impaired osteoclast formation, and thereby attenuated bone resorption.[22] The two investigated affected individuals showed a trend toward lower circulating RANKL/OPG ratios.

Moreover, canonical Wnt signaling influences cartilage growth and differentiation and thereby longitudinal and lateral expansion of the columnar cartilage in the growth plate.[43] It seems likely that the hip dysplasia in five of the six comprehensively documented affected individuals is due to an altered growth at the proximal femur. Overexpression of *Ctnnb1* in hypertrophic chondrocytes led to a

prominent expansion of the mineralized cartilage at the resorption zone of the growth plate as a consequence of a lower Rankl/Opg-ratio and impaired osteoclast recruitment.[44] Thus, in contrast to osteopetrosis, the growth plate sclerosis in long bones and vertebrae in the *AXIN1*-related sclerosing skeletal dysplasia could be rather a consequence of a local, not a generalized, osteoclast dysregulation.

Intriguingly, the *AXIN1* variants we identified in all four families were within the last 3 exons of the gene. Full deletion of *Axin1* was demonstrated to lead to embryonic death in mice, implying that only congenital variants mildly affecting AXIN1 function are tolerated in living organisms.[21] Indeed, fibroblasts of an affected individual as well as genome-edited cell lines display residual AXIN1 levels and partially retained regulatory capacity in the Wnt pathway, suggesting that these variants belong to a class of hypomorphic AXIN1 alterations distinct from loss-of-function variants. Nonetheless, loss of the C-terminal DIX domain is suspected to have considerable consequences for AXIN1 function. This multifaceted domain is required for its self-polymerization, as was clearly observed in our immunofluorescence analysis, but it also mediates translocation of AXIN1 to the plasma membrane via its interaction with DVL. We therefore envision that the paralog *AXIN2* partially compensates for the *AXIN1* variants within these affected individuals. Indeed, we observed upregulation of *AXIN2* in some of the *AXIN1*-mutant HEK293T lines as well as in primary fibroblasts.

In the last decades, several studies reported an association between loss of AXIN1 and cancerogenesis.[24,45] Truncating *AXIN1* somatic variants are frequently identified in different subsets of tumors, most notably in hepatocellular carcinoma and endometrial carcinoma.[46] Since the description of the destruction-complex-related OS-CS, five instances of childhood cancer in females with OS-CS (four Wilms tumor, one hepatoblastoma) and two adult-onset cancer (colorectal, ovarian) have been reported.[33,34,47–49] While no tumors have been observed in the individuals of this study, these findings indicate that monitoring of individuals with *AXIN1*-truncating variants may be warranted.

In aggregate, we describe a sclerosing bone dysplasia with evidence of increased osteoblast and reduced osteoclast function at the growth plate's resorption zone leading to coarse trabeculae. We propose to designate this condition as "Craniometadiaphyseal osteosclerosis with hip dysplasia, *AXIN1*-related" in the nosology of skeletal disorders.[50] All causative variants lead to a truncation of AXIN1 affecting the DIX domain. The reduced protein levels and impaired AXIN1 polymerization leads to enhanced canonical Wnt signaling, which could be attenuated by tankyrase inhibition.

Data and code availability

The published article includes all datasets generated or analyzed during this study. The exome-sequencing data of the four families supporting the current study have not been deposited in a public repository because of privacy issues but are available from the corresponding author on request.

Supplemental information

Supplemental information can be found online at https://doi.org/10.1016/j.ajhg.2023.07.011.

Acknowledgments

We gratefully acknowledge the affected individuals and their parents for their cooperation in this study. We thank Henrietta Lacks (donor of the cervical cancer cell line HeLa) and her family for their contribution to research. We thank Chris van Kesteren for help with the illustrations. We thank Enya Vermeulen for technical laboratory assistance. We thank Koen van Gassen and Gijs van Haaften for performing the DNA tests in the DNA laboratory and Professor Bram van der Eerden and Marijke Koedam for assessment of RANKL/OPG levels in family 1. We thank Antonia Howaldt for immunoblots. U.K. received funding from the German Federal Ministry of Education and Research (BMBF) (031L0234A "BOAC"), the Elsbeth Bonhoff Stiftung (Zuwendungsgesuch 98), and the German Research Foundation (DFG) (KO2891/9-1).

Author contributions

P.T., A.V., M.M., and U.K. wrote the manuscript. P.T., D.L., E.N., W.-H.T., A.A., H.I.A., P.B., T.K., M.H., C.K., A.B.-A., and A.v.D. provided clinical and genetic data, which was collected by P.T. R.A.J.N. and U.K. reviewed the radiographs. A.V., R.G., A.C., and N.R. performed the bulk of experiments and analyzed the results. H.H., M.M., B.F.-Z., and U.K. supervised the experiments and interpreted the results. P.N., S.v.K., and R.O. performed anatomical pathological examination of bone biopsies and discussed the results. All authors discussed results and commented on the manuscript.

Declaration of interests

The authors declare no competing interests.

Received: April 7, 2023
Accepted: July 26, 2023
Published: August 14, 2023

Web resources

GeneMatcher, https://genematcher.org
GnomadAD, https://gnomad.broadinstitute.org/
ImageJ, https://imagej.nih.gov/
OMIM, https://omim.org
Synthego CRISPR editing prediction tool, https://ice.synthego.com

References

1. De Ridder, R., Boudin, E., Mortier, G., and Van Hul, W. (2018). Human Genetics of Sclerosing Bone Disorders. Curr. Osteoporos. Rep. *16*, 256–268.
2. de Vernejoul, M.C., and Kornak, U. (2010). Heritable sclerosing bone disorders: presentation and new molecular mechanisms. Ann. N. Y. Acad. Sci. *1192*, 269–277.

3. Baron, R., and Kneissel, M. (2013). WNT signaling in bone homeostasis and disease: from human mutations to treatments. Nat. Med. *19*, 179–192.
4. Keupp, K., Beleggia, F., Kayserili, H., Barnes, A.M., Steiner, M., Semler, O., Fischer, B., Yigit, G., Janda, C.Y., Becker, J., et al. (2013). Mutations in WNT1 cause different forms of bone fragility. Am. J. Hum. Genet. *92*, 565–574.
5. Laine, C.M., Joeng, K.S., Campeau, P.M., Kiviranta, R., Tarkkonen, K., Grover, M., Lu, J.T., Pekkinen, M., Wessman, M., Heino, T.J., et al. (2013). WNT1 mutations in early-onset osteoporosis and osteogenesis imperfecta. N. Engl. J. Med. *368*, 1809–1816.
6. Luther, J., Yorgan, T.A., Rolvien, T., Ulsamer, L., Koehne, T., Liao, N., Keller, D., Vollersen, N., Teufel, S., Neven, M., et al. (2018). Wnt1 is an Lrp5-independent bone-anabolic Wnt ligand. Sci. Transl. Med. *10*, eaau7137. https://doi.org/10.1126/scitranslmed.aau7137.
7. Boyden, L.M., Mao, J., Belsky, J., Mitzner, L., Farhi, A., Mitnick, M.A., Wu, D., Insogna, K., and Lifton, R.P. (2002). High bone density due to a mutation in LDL-receptor-related protein 5. N. Engl. J. Med. *346*, 1513–1521.
8. Gong, Y., Slee, R.B., Fukai, N., Rawadi, G., Roman-Roman, S., Reginato, A.M., Wang, H., Cundy, T., Glorieux, F.H., Lev, D., et al. (2001). LDL receptor-related protein 5 (LRP5) affects bone accrual and eye development. Cell *107*, 513–523.
9. Mani, A., Radhakrishnan, J., Wang, H., Mani, A., Mani, M.A., Nelson-Williams, C., Carew, K.S., Mane, S., Najmabadi, H., Wu, D., and Lifton, R.P. (2007). LRP6 mutation in a family with early coronary disease and metabolic risk factors. Science *315*, 1278–1282.
10. Whyte, M.P., McAlister, W.H., Zhang, F., Bijanki, V.N., Nenninger, A., Gottesman, G.S., Lin, E.L., Huskey, M., Duan, S., Dahir, K., and Mumm, S. (2019). New explanation for autosomal dominant high bone mass: Mutation of low-density lipoprotein receptor-related protein 6. Bone *127*, 228–243.
11. Stamos, J.L., and Weis, W.I. (2013). The beta-catenin destruction complex. Cold Spring Harb. Perspect. Biol. *5*, a007898.
12. Teufel, S., and Hartmann, C. (2019). Wnt-signaling in skeletal development. Curr. Top. Dev. Biol. *133*, 235–279.
13. Sato, M.M., Nakashima, A., Nashimoto, M., Yawaka, Y., and Tamura, M. (2009). Bone morphogenetic protein-2 enhances Wnt/beta-catenin signaling-induced osteoprotegerin expression. Gene Cell. *14*, 141–153.
14. Albers, J., Keller, J., Baranowsky, A., Beil, F.T., Catala-Lehnen, P., Schulze, J., Amling, M., and Schinke, T. (2013). Canonical Wnt signaling inhibits osteoclastogenesis independent of osteoprotegerin. J. Cell Biol. *200*, 537–549.
15. van Kappel, E.C., and Maurice, M.M. (2017). Molecular regulation and pharmacological targeting of the beta-catenin destruction complex. Br. J. Pharmacol. *174*, 4575–4588.
16. Spink, K.E., Polakis, P., and Weis, W.I. (2000). Structural basis of the Axin-adenomatous polyposis coli interaction. EMBO J. *19*, 2270–2279.
17. Schwarz-Romond, T., Fiedler, M., Shibata, N., Butler, P.J.G., Kikuchi, A., Higuchi, Y., and Bienz, M. (2007). The DIX domain of Dishevelled confers Wnt signaling by dynamic polymerization. Nat. Struct. Mol. Biol. *14*, 484–492.
18. Kishida, S., Yamamoto, H., Hino, S., Ikeda, S., Kishida, M., and Kikuchi, A. (1999). DIX domains of Dvl and axin are necessary for protein interactions and their ability to regulate beta-catenin stability. Mol. Cell Biol. *19*, 4414–4422.
19. Hamada, F., Tomoyasu, Y., Takatsu, Y., Nakamura, M., Nagai, S., Suzuki, A., Fujita, F., Shibuya, H., Toyoshima, K., Ueno, N., and Akiyama, T. (1999). Negative regulation of Wingless signaling by D-axin, a Drosophila homolog of axin. Science *283*, 1739–1742.
20. Heisenberg, C.P., Houart, C., Take-Uchi, M., Rauch, G.J., Young, N., Coutinho, P., Masai, I., Caneparo, L., Concha, M.L., Geisler, R., et al. (2001). A mutation in the Gsk3-binding domain of zebrafish Masterblind/Axin1 leads to a fate transformation of telencephalon and eyes to diencephalon. Genes Dev. *15*, 1427–1434.
21. Perry, W.L., 3rd, Vasicek, T.J., Lee, J.J., Rossi, J.M., Zeng, L., Zhang, T., Tilghman, S.M., and Costantini, F. (1995). Phenotypic and molecular analysis of a transgenic insertional allele of the mouse Fused locus. Genetics *141*, 321–332.
22. Shu, B., Zhao, Y., Zhao, S., Pan, H., Xie, R., Yi, D., Lu, K., Yang, J., Xue, C., Huang, J., et al. (2020). Inhibition of Axin1 in osteoblast precursor cells leads to defects in postnatal bone growth through suppressing osteoclast formation. Bone Res. *8*, 31–35. eCollection 2020.
23. Fiedler, M., Mendoza-Topaz, C., Rutherford, T.J., Mieszczanek, J., and Bienz, M. (2011). Dishevelled interacts with the DIX domain polymerization interface of Axin to interfere with its function in down-regulating beta-catenin. Proc. Natl. Acad. Sci. USA *108*, 1937–1942.
24. Abitbol, S., Dahmani, R., Coulouarn, C., Ragazzon, B., Mlecnik, B., Senni, N., Savall, M., Bossard, P., Sohier, P., Drouet, V., et al. (2018). AXIN deficiency in human and mouse hepatocytes induces hepatocellular carcinoma in the absence of beta-catenin activation. J. Hepatol. *68*, 1203–1213.
25. Anvarian, Z., Nojima, H., van Kappel, E.C., Madl, T., Spit, M., Viertler, M., Jordens, I., Low, T.Y., van Scherpenzeel, R.C., Kuper, I., et al. (2016). Axin cancer mutants form nanoaggregates to rewire the Wnt signaling network. Nat. Struct. Mol. Biol. *23*, 324–332.
26. Tauriello, D.V.F., Haegebarth, A., Kuper, I., Edelmann, M.J., Henraat, M., Canninga-van Dijk, M.R., Kessler, B.M., Clevers, H., and Maurice, M.M. (2010). Loss of the tumor suppressor CYLD enhances Wnt/beta-catenin signaling through K63-linked ubiquitination of Dvl. Mol. Cell *37*, 607–619.
27. Ran, F.A., Hsu, P.D., Wright, J., Agarwala, V., Scott, D.A., and Zhang, F. (2013). Genome engineering using the CRISPR-Cas9 system. Nat. Protoc. *8*, 2281–2308.
28. Pospisil, H., Herrmann, A., Butherus, K., Pirson, S., Reich, J.G., and Kemmner, W. (2006). Verification of predicted alternatively spliced Wnt genes reveals two new splice variants (CTNNB1 and LRP5) and altered Axin-1 expression during tumour progression. BMC Genom. *7*, 148.
29. Karczewski, K.J., Francioli, L.C., Tiao, G., Cummings, B.B., Alföldi, J., Wang, Q., Collins, R.L., Laricchia, K.M., Ganna, A., Birnbaum, D.P., et al. (2020). The mutational constraint spectrum quantified from variation in 141,456 humans. Nature *581*, 434–443.
30. Dao, D.Y., Yang, X., Chen, D., Zuscik, M., and O'Keefe, R.J. (2007). Axin1 and Axin2 are regulated by TGF- and mediate cross-talk between TGF- and Wnt signaling pathways. Ann. N. Y. Acad. Sci. *1116*, 82–99.
31. Schwarz-Romond, T., Metcalfe, C., and Bienz, M. (2007). Dynamic recruitment of axin by Dishevelled protein assemblies. J. Cell Sci. *120*, 2402–2412.
32. Huang, S.M.A., Mishina, Y.M., Liu, S., Cheung, A., Stegmeier, F., Michaud, G.A., Charlat, O., Wiellette, E., Zhang, Y.,

Wiessner, S., et al. (2009). Tankyrase inhibition stabilizes axin and antagonizes Wnt signalling. Nature *461*, 614–620.
33. Jenkins, Z.A., van Kogelenberg, M., Morgan, T., Jeffs, A., Fukuzawa, R., Pearl, E., Thaller, C., Hing, A.V., Porteous, M.E., Garcia-Miñaur, S., et al. (2009). Germline mutations in WTX cause a sclerosing skeletal dysplasia but do not predispose to tumorigenesis. Nat. Genet. *41*, 95–100.
34. Perdu, B., de Freitas, F., Frints, S.G.M., Schouten, M., Schrander-Stumpel, C., Barbosa, M., Pinto-Basto, J., Reis-Lima, M., de Vernejoul, M.C., Becker, K., et al. (2010). Osteopathia striata with cranial sclerosis owing to WTX gene defect. J. Bone Miner. Res. *25*, 82–90.
35. Bunn, K.J., Daniel, P., Rösken, H.S., O'Neill, A.C., Cameron-Christie, S.R., Morgan, T., Brunner, H.G., Lai, A., Kunst, H.P.M., Markie, D.M., and Robertson, S.P. (2015). Mutations in DVL1 cause an osteosclerotic form of Robinow syndrome. Am. J. Hum. Genet. *96*, 623–630.
36. Ward, L.M., Rauch, F., Travers, R., Roy, M., Montes, J., Chabot, G., and Glorieux, F.H. (2004). Osteopathia striata with cranial sclerosis: clinical, radiological, and bone histological findings in an adolescent girl. Am. J. Med. Genet. *129A*, 8–12.
37. Shayota, B.J., Zhang, C., Shypailo, R.J., Mazzeu, J.F., Carvalho, C.M.B., and Sutton, V.R. (2020). Characterization of the Robinow syndrome skeletal phenotype, bone micro-architecture, and genotype-phenotype correlations with the osteosclerotic form. Am. J. Med. Genet. *182*, 2632–2640.
38. Sobacchi, C., Schulz, A., Coxon, F.P., Villa, A., and Helfrich, M.H. (2013). Osteopetrosis: genetics, treatment and new insights into osteoclast function. Nat. Rev. Endocrinol. *9*, 522–536.
39. Sobacchi, C., Villa, A., Schulz, A., and Kornak, U. (1993). CLCN7-Related Osteopetrosis. In GeneReviews((R)), M.P. Adam, G.M. Mirzaa, R.A. Pagon, S.E. Wallace, L.J.H. Bean, K.W. Gripp, and A. Amemiya, eds. (University of Washington).
40. Albers, J., Schulze, J., Beil, F.T., Gebauer, M., Baranowsky, A., Keller, J., Marshall, R.P., Wintges, K., Friedrich, F.W., Priemel, M., et al. (2011). Control of bone formation by the serpentine receptor Frizzled-9. J. Cell Biol. *192*, 1057–1072.
41. Day, T.F., Guo, X., Garrett-Beal, L., and Yang, Y. (2005). Wnt/beta-catenin signaling in mesenchymal progenitors controls osteoblast and chondrocyte differentiation during vertebrate skeletogenesis. Dev. Cell *8*, 739–750.
42. Glass, D.A., 2nd, Bialek, P., Ahn, J.D., Starbuck, M., Patel, M.S., Clevers, H., Taketo, M.M., Long, F., McMahon, A.P., Lang, R.A., and Karsenty, G. (2005). Canonical Wnt signaling in differentiated osteoblasts controls osteoclast differentiation. Dev. Cell *8*, 751–764.
43. Oichi, T., Otsuru, S., Usami, Y., Enomoto-Iwamoto, M., and Iwamoto, M. (2020). Wnt signaling in chondroprogenitors during long bone development and growth. Bone *137*, 115368.
44. Houben, A., Kostanova-Poliakova, D., Weissenböck, M., Graf, J., Teufel, S., von der Mark, K., and Hartmann, C. (2016). Beta-Catenin Activity in Late Hypertrophic Chondrocytes Locally Orchestrates Osteoblastogenesis and Osteoclastogenesis. Development *143*, 3826–3838.
45. Satoh, S., Daigo, Y., Furukawa, Y., Kato, T., Miwa, N., Nishiwaki, T., Kawasoe, T., Ishiguro, H., Fujita, M., Tokino, T., et al. (2000). AXIN1 mutations in hepatocellular carcinomas, and growth suppression in cancer cells by virus-mediated transfer of AXIN1. Nat. Genet. *24*, 245–250.
46. Bugter, J.M., Fenderico, N., and Maurice, M.M. (2021). Publisher Correction: Mutations and mechanisms of WNT pathway tumour suppressors in cancer. Nat. Rev. Cancer *21*, 64–y.
47. Sperotto, F., Bisogno, G., Opocher, E., Rossi, S., Rigon, C., Trevisson, E., and Mercolini, F. (2017). Osteopathia striata with cranial sclerosis and Wilms tumor: Coincidence or consequence? Clin. Genet. *92*, 674–675.
48. Bach, A., Mi, J., Hunter, M., Halliday, B.J., García-Miñaúr, S., Sperotto, F., Trevisson, E., Markie, D., Morison, I.M., Shinawi, M., et al. (2021). Wilms tumor in patients with osteopathia striata with cranial sclerosis. Eur. J. Hum. Genet. *29*, 396–401.
49. Fujita, A., Ochi, N., Fujimaki, H., Muramatsu, H., Takahashi, Y., Natsume, J., Kojima, S., Nakashima, M., Tsurusaki, Y., Saitsu, H., et al. (2014). A novel WTX mutation in a female patient with osteopathia striata with cranial sclerosis and hepatoblastoma. Am. J. Med. Genet. *164A*, 998–1002.
50. Unger, S., Ferreira, C.R., Mortier, G.R., Ali, H., Bertola, D.R., Calder, A., Cohn, D.H., Cormier-Daire, V., Girisha, K.M., Hall, C., et al. (2023). Nosology of genetic skeletal disorders: 2023 revision. Am. J. Med. Genet. *191*, 1164–1209.